Emulator-Assisted Investigation of Left-Right Symmetric Higgs Inflation

Mehraveh Nikjoo, Tom Zlosnik

June 29, 2026

Exordium

One fundamental issue

Small anisotropies of CMB exhibit a statistically coherent pattern across the sky.

Encoded in the angular power spectrum,

$$\left\langle \frac{\Delta T}{T}(\hat{n})\, \frac{\Delta T}{T}(\hat{n}') \right\rangle = \sum_{\ell} \frac{2\ell+1}{4\pi}\, C_\ell\, P_\ell(\hat{n}\cdot\hat{n}').$$

Inflation provides the causal mechanism behind this structure: quantum fluctuations generated during an early accelerated phase are stretched beyond the Hubble radius and later re-enter as classical perturbations, sourcing the observed CMB anisotropies and the large-scale distribution of matter.

Preamble

Matter sector

- The weak interaction distinguishes left- and right-handed fermions.

Gravitational sector

Preamble

Matter sector

- The weak interaction distinguishes left- and right-handed fermions.
- Left–right symmetry interprets this asymmetry as the remnant of a broken high-energy symmetry.

Gravitational sector

Preamble

Matter sector

- The weak interaction distinguishes left- and right-handed fermions.
- Left–right symmetry interprets this asymmetry as the remnant of a broken high-energy symmetry.

$$SU(2)_L \times SU(2)_R \times U(1)_{B-L} \longrightarrow SU(2)_L \times U(1)_Y$$

Gravitational sector

Preamble

Matter sector

- The weak interaction distinguishes left- and right-handed fermions.
- Left–right symmetry interprets this asymmetry as the remnant of a broken high-energy symmetry.

$$SU(2)_L \times SU(2)_R \times U(1)_{B-L} \longrightarrow SU(2)_L \times U(1)_Y$$

Gravitational sector

- The Lorentz connection admits a chiral decomposition into self-dual and anti-self-dual parts.

Preamble

Matter sector

- The weak interaction distinguishes left- and right-handed fermions.
- Left–right symmetry interprets this asymmetry as the remnant of a broken high-energy symmetry.

$$SU(2)_L \times SU(2)_R \times U(1)_{B-L} \longrightarrow SU(2)_L \times U(1)_Y$$

Gravitational sector

- The Lorentz connection admits a chiral decomposition into self-dual and anti-self-dual parts.

$$\mathfrak{so}(1,3)_{\mathbb{C}} \tilde{=} \mathfrak{sl}(2)_{\mathbb{C}} \oplus \mathfrak{sl}(2)_{\mathbb{C}}$$

Preamble

Matter sector

- The weak interaction distinguishes left- and right-handed fermions.
- Left–right symmetry interprets this asymmetry as the remnant of a broken high-energy symmetry.

$$SU(2)_L \times SU(2)_R \times U(1)_{B-L} \longrightarrow SU(2)_L \times U(1)_Y$$

Gravitational sector

- The Lorentz connection admits a chiral decomposition into self-dual and anti-self-dual parts.

$$\mathfrak{so}(1,3)_{\mathbb{C}} \tilde{=} \mathfrak{sl}(2)_{\mathbb{C}} \oplus \mathfrak{sl}(2)_{\mathbb{C}}$$

$$\omega^{IJ} = \omega^{+IJ} + \omega^{-IJ}$$

Model background: first-order gravity in gauge theory language

- Metric is reconstructed from the co-tetrad:

$$g_{\mu\nu} = \eta_{IJ} e^I_\mu e^J_\nu$$

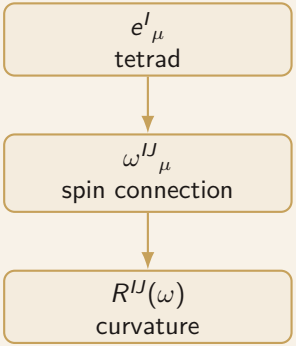

Model background: first-order gravity in gauge theory language

- Metric is reconstructed from the co-tetrad:

$$g_{\mu\nu} = \eta_{IJ} e^I_\mu e^J_\nu$$

- Any antisymmetric Lorentz tensor admits an internal Hodge dual:

$$F^{IJ} = -F^{JI}, \qquad (\star F)^{IJ} = \frac{1}{2}\epsilon^{IJ}{}_{KL} F^{KL}$$

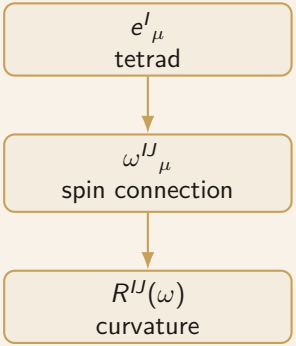

Model background: first-order gravity in gauge theory language

- Metric is reconstructed from the co-tetrad:

$$g_{\mu\nu} = \eta_{IJ} e^I_\mu e^J_\nu$$

- Any antisymmetric Lorentz tensor admits an internal Hodge dual:

$$F^{IJ} = -F^{JI}, \qquad (\star F)^{IJ} = \frac{1}{2}\epsilon^{IJ}{}_{KL} F^{KL}$$

- After complexification, this defines the chiral projections:

$$F^{\pm IJ} = \frac{1}{2}\left(F^{IJ} \mp i(\star F)^{IJ}\right) = \frac{1}{2}\left(F^{IJ} \mp \frac{i}{2}\epsilon^{IJ}{}_{KL} F^{KL}\right) \equiv \omega^{\pm IJ}$$

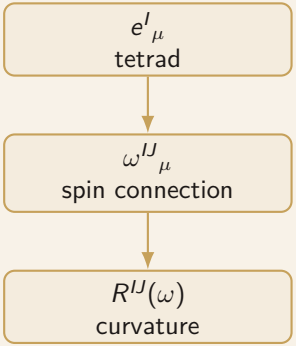

Model background: Left–right symmetric Higgs sector

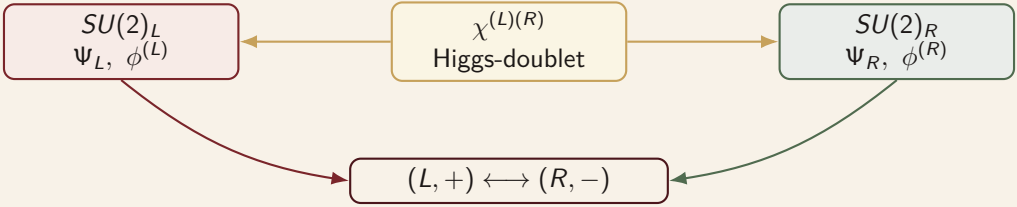

Model

$$\mathcal{L}_G = \frac{1}{32\pi G}\,\epsilon_{IJKL}\,e^I \wedge e^J \wedge R^{KL}(\omega) + \mathcal{L}^{\mathrm{LR}}_{\mathrm{NM}}$$

Model

$$\mathcal{L}_G = \frac{1}{32\pi G}\,\epsilon_{IJKL}\,e^I \wedge e^J \wedge R^{KL}(\omega) + \mathcal{L}^{\mathrm{LR}}_{\mathrm{NM}}$$

$$= \frac{\overline{M}_{\mathrm{Pl}}^2}{4}\left(\epsilon_{IJKL} + \frac{2}{\overline{\gamma}}\eta_{IK}\eta_{JL}\right) e^I \wedge e^J \wedge R^{KL}(\omega).$$

Model

$$\mathcal{L}_G = \frac{1}{32\pi G}\,\epsilon_{IJKL}\,e^I \wedge e^J \wedge R^{KL}(\omega) + \mathcal{L}^{\mathrm{LR}}_{\mathrm{NM}}$$
$$= \frac{\overline{M}_{\mathrm{Pl}}^2}{4}\left(\epsilon_{IJKL} + \frac{2}{\overline{\gamma}}\eta_{IK}\eta_{JL}\right) e^I \wedge e^J \wedge R^{KL}(\omega).$$

Effective Planck mass

$$\overline{M}_{\mathrm{Pl}}^2 = \frac{1}{8\pi G} + \xi_1\,\chi^\dagger\chi + \xi_2\,\mathrm{Re}[\det(\chi)] + \xi_3\,\mathrm{Im}[\det(\chi)]$$
$$+ (\zeta + \eta)\left(\phi^{(R)}\cdot\phi^{(R)} + \phi^{(L)}\cdot\phi^{(L)}\right).$$

Model

$$\mathcal{L}_G = \frac{1}{32\pi G}\,\epsilon_{IJKL}\,e^I \wedge e^J \wedge R^{KL}(\omega) + \mathcal{L}^{\mathrm{LR}}_{\mathrm{NM}}$$

$$= \frac{\overline{M}^2_{\mathrm{Pl}}}{4}\left(\epsilon_{IJKL} + \frac{2}{\overline{\gamma}}\eta_{IK}\eta_{JL}\right) e^I \wedge e^J \wedge R^{KL}(\omega).$$

Effective Planck mass

$$\overline{M}^2_{\mathrm{Pl}} = \frac{1}{8\pi G} + \xi_1\,\chi^\dagger\chi + \xi_2\,\mathrm{Re}[\det(\chi)] + \xi_3\,\mathrm{Im}[\det(\chi)] + (\zeta+\eta)\left(\phi^{(R)}\cdot\phi^{(R)} + \phi^{(L)}\cdot\phi^{(L)}\right).$$

Effective Barbero–Immirzi parameter

$$\overline{\gamma} = -i\,\frac{\overline{M}^2_{\mathrm{Pl}}}{(\zeta-\eta)\left(\phi^{(L)}\cdot\phi^{(L)} - \phi^{(R)}\cdot\phi^{(R)}\right)}.$$

Model assumption: single-field trajectory

$$\phi^{(R)} \overset{SU(2)_R}{\sim} (0, 0, \phi)$$

Model assumption: single-field trajectory

$$\phi^{(R)} \overset{SU(2)_R}{\sim} (0, 0, \phi)$$

$$\mathcal{L} = \bar{a}^3 \bar{N} \left[-3M_{\rm Pl}^2 \frac{\dot{\bar{a}}^2}{\bar{N}^2 \bar{a}^2} + Y(\phi) \frac{\dot{\phi}^2}{\bar{N}^2} - \frac{V(\phi)}{V_0(\phi)^2} \right]$$

Model assumption: single-field trajectory

$$\phi^{(R)} \overset{SU(2)_R}{\sim} (0, 0, \phi)$$

$$\mathcal{L} = \bar{a}^3 \bar{N} \left[-3M_{\rm Pl}^2 \frac{\dot{\bar{a}}^2}{\bar{N}^2 \bar{a}^2} + Y(\phi) \frac{\dot{\phi}^2}{\bar{N}^2} - \frac{V(\phi)}{V_0(\phi)^2} \right]$$

$$Y(\phi) = \frac{1}{V_0} \left[1 + \frac{3}{1 + \bar{\gamma}^2} \frac{1}{V_0} \frac{M_{\rm Pl}^2}{\phi^2} \right]$$

Model assumption: single-field trajectory

$$\phi^{(R)} \overset{SU(2)_R}{\sim} (0, 0, \phi)$$

$$\mathcal{L} = \bar{a}^3 \bar{N} \left[-3M_{\rm Pl}^2 \frac{\dot{\bar{a}}^2}{\bar{N}^2 \bar{a}^2} + Y(\phi) \frac{\dot{\phi}^2}{\bar{N}^2} - \frac{V(\phi)}{V_0(\phi)^2} \right]$$

$$Y(\phi) = \frac{1}{V_0} \left[1 + \frac{3}{1 + \bar{\gamma}^2} \frac{1}{V_0} \frac{M_{\rm Pl}^2}{\phi^2} \right]$$

$$V_0(\phi) = 1 + (\zeta + \eta) \frac{\phi^2}{M_{\rm Pl}^2}$$

Model assumption: single-field trajectory

$$\phi^{(R)} \overset{SU(2)_R}{\sim} (0, 0, \phi)$$

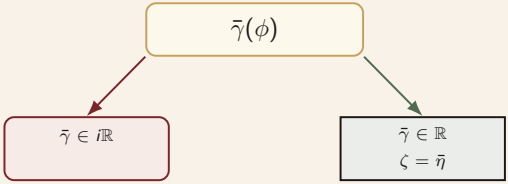

$$\mathcal{L} = \bar{a}^3 \bar{N} \left[-3M_{\rm Pl}^2 \frac{\dot{\bar{a}}^2}{\bar{N}^2 \bar{a}^2} + Y(\phi) \frac{\dot{\phi}^2}{\bar{N}^2} - \frac{V(\phi)}{V_0(\phi)^2} \right]$$

$$Y(\phi) = \frac{1}{V_0} \left[1 + \frac{3}{1+\bar{\gamma}^2} \frac{1}{V_0} \frac{M_{\rm Pl}^2}{\phi^2} \right]$$

$$V_0(\phi) = 1 + (\zeta + \eta) \frac{\phi^2}{M_{\rm Pl}^2}$$

Perturbations

Perturbation ansatz

$$\delta\bar{e}^{\,0} = \Psi\,\bar{E}^{0} + L_i\,\bar{E}^{i},$$
$$\delta\bar{e}^{\,i} = N^{i}\,\bar{E}^{0} + S^{ij}\bar{E}^{j}$$

$$\delta\omega^{0i} = \gamma^{i}\bar{E}^{0} + \xi\,\bar{E}^{i} + \epsilon^{ijk}\mu^{j}\bar{E}^{k} + \tau^{ij}\bar{E}^{j},$$
$$\delta\omega^{ij} = \epsilon^{ij}{}_{k}\varphi^{k}\bar{E}^{0} + \zeta\,\epsilon^{ij}{}_{k}\bar{E}^{k} + \nu^{[i}\bar{E}^{j]} + \epsilon^{ij}{}_{k}\chi^{kl}\bar{E}^{l}$$

Scalar-vector-tensor decomposition

$$L_i = \partial_i L$$

$$S_{ij} = \frac{1}{3}\,h\,\delta_{ij} + \left(\partial_i\partial_j - \frac{1}{3}\delta_{ij}\partial^2\right) S + \epsilon_{ijk}\partial_k A$$

Gauge choice

$$\delta\phi \overset{*}{=} 0, \qquad S \overset{*}{=} 0$$

Perturbations: scalar sector

Mukhanov–Sasaki form

$$S_S[\tilde{\nu}] = \frac{1}{2}\int d\tau\, d^3k\, \left[\tilde{\nu}^{*\prime}\tilde{\nu}' - \left(k^2 - \frac{Z''}{Z}\right)\tilde{\nu}^*\tilde{\nu}\right]$$

Canonical normalization

$$\bar{N} = \bar{a}, \qquad \tilde{\nu} = \frac{Z}{3}h$$

$$Z^2 = \frac{2\bar{a}^2\, Y(\phi)\, \phi'^2}{(\bar{a}'/\bar{a})^2}$$

Perturbations: tensor sector

Relevant tensor fields

$$h_{ij} = S_{ij}\big|_{\mathrm{STT}}, \qquad B_{ij} = \frac{1}{\bar{\gamma}\,\bar{a}^2}\left(\chi_{ij} + \bar{\gamma}\,\tau_{ij}\right)\Big|_{\mathrm{STT}}$$

Tensor action

$$S_T[h, B] = \int dt\, d^3x\, \mathcal{L}_T$$

$$\mathcal{L}_T = -\,M_{\mathrm{Pl}}^2\,\bar{a}\,h_{ij}\,\dot{B}^{ij} - \mathcal{H}(h, B)$$

Hamiltonian structure

$$\mathcal{H} = \mathcal{H}\big(h_{ij},\, B_{ij},\, \partial_k h_{ij},\, \partial_k B_{ij}\big)$$

The tensor sector formulated as a first-order system in the pair

$$(h_{ij},\, B_{ij}).$$

In contrast with the scalar sector, the connection perturbation survives explicitly, so the first-order chiral structure remains visible at tensor level.

Perturbations: tensor sector

Relevant tensor fields

$$h_{ij} = S_{ij}\big|_{\mathrm{STT}}, \quad B_{ij} = \frac{1}{\bar{\gamma}\,\bar{a}^2}\left(\chi_{ij} + \bar{\gamma}\,\tau_{ij}\right)\Big|_{\mathrm{STT}}$$

Tensor action

$$S_T[h, B] = \int dt\, d^3x\, \mathcal{L}_T$$

$$\mathcal{L}_T = -\,M_{\mathrm{Pl}}^2\,\bar{a}\,h_{ij}\,\dot{B}^{ij} - \mathcal{H}(h, B)$$

The equations of motion for B_{ij} are algebraic. Solving them and substituting back gives

$$S_T[h] = \frac{M_{\mathrm{Pl}}^2}{2}\int d\tau\, d^3x\, \bar{a}^2\left(h'_{ij}h'^{ij} - \partial_k h_{ij}\partial^k h^{ij}\right)$$

We recover the standard tensor action on the FLRW background.

Numerical development: sampled parameters and likelihood

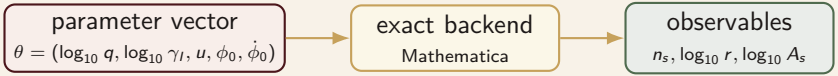

Numerical development: sampled parameters and likelihood

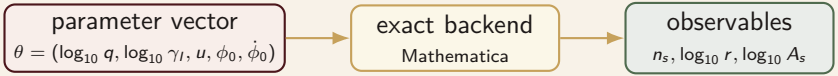

Parameter domain

$\log_{10} q \in [-10, 10]$, $\log_{10} \gamma_I \in [-1, 10]$,
$u \in [-11.5, -10.0]$, $\phi_0 \in [10, 20]$,
$\dot{\phi}_0 \in [-0.1, 0.1]$, $u = \log_{10}\left(\frac{\lambda}{q}\right)$.

Here $q = \zeta + \eta$ controls the overall non-minimal coupling scale.

Numerical development: sampled parameters and likelihood

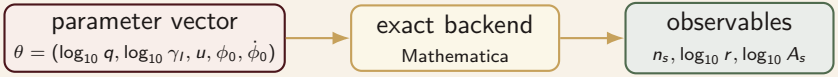

Parameter domain

$\log_{10} q \in [-10, 10]$, $\log_{10} \gamma_I \in [-1, 10]$,
$u \in [-11.5, -10.0]$, $\phi_0 \in [10, 20]$,
$\dot{\phi}_0 \in [-0.1, 0.1]$, $u = \log_{10}\left(\frac{\lambda}{q}\right)$.

Here $q = \zeta + \eta$ controls the overall non-minimal coupling scale.

Posterior likelihood

$$\ln \mathcal{L}(\theta) = -\frac{1}{2}\left[\frac{n_s(\theta) - n_s^{\rm obs}}{\sigma_{n_s,\rm eff}}\right]^2 - \frac{1}{2}\left[\frac{\log_{10} A_s(\theta) - \log_{10} A_s^{\rm obs}}{\sigma_{\log_{10} A_s,\rm eff}}\right]^2.$$

$$r(\theta) < 0.06, \qquad \sigma^2_{\rm eff} = \sigma^2_{\rm obs} + \sigma^2_{\rm emu}.$$

Numerical pipeline

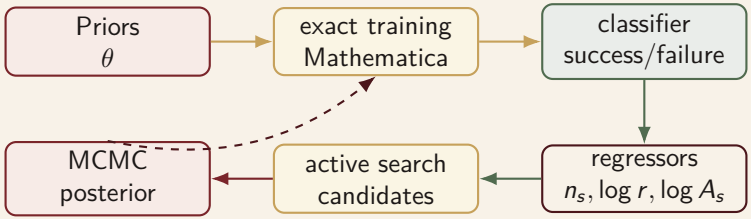

Observational landing point

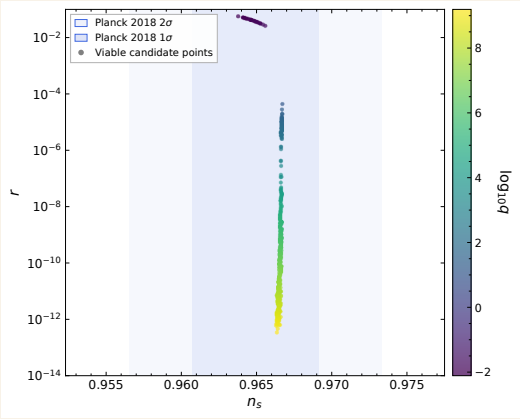

$\bar{\gamma} \in i\mathbb{R}$.

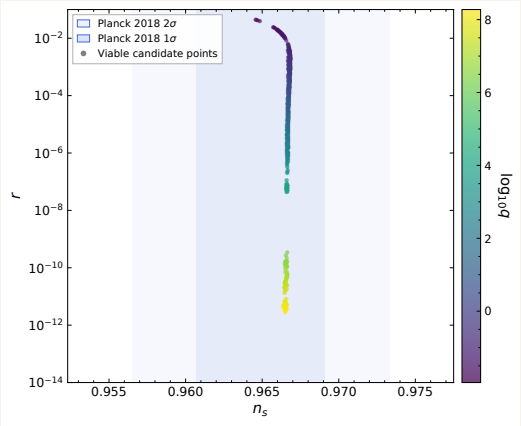

$\bar{\gamma} \in \mathbb{R}$.

Imaginary branch: response to $\bar{\gamma}_I$

Test performed: all parameters are fixed at their posterior median values, while

$$\log_{10} \bar{\gamma}_I$$

is varied across its prior range.

Imaginary branch: response to $\bar{\gamma}_I$

Test performed: all parameters are fixed at their posterior median values, while

$$\log_{10} \bar{\gamma}_I$$

is varied across its prior range.

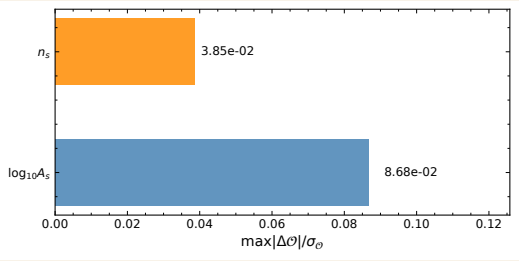

Planck-normalized response of n_s and $\log_{10} A_s$.

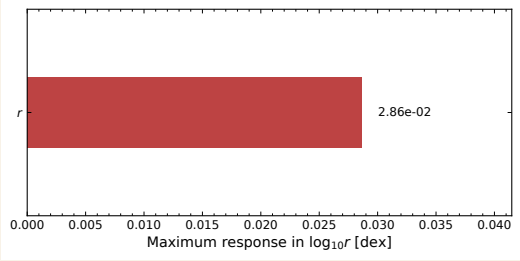

Response of the tensor amplitude, shown as a shift in $\log_{10} r$.

Imaginary branch: $\bar{\gamma}_I$ posterior

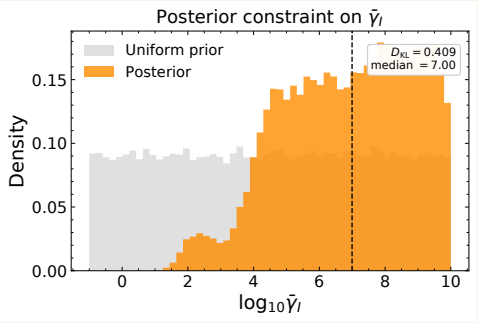

Posterior distribution of $\log_{10} \bar{\gamma}_I$.

Imaginary branch: $\bar{\gamma}_I$ posterior

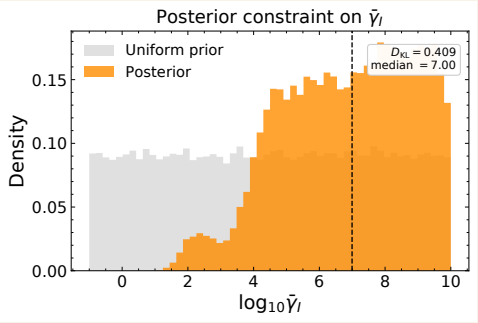

Posterior distribution of $\log_{10}\bar{\gamma}_I$.

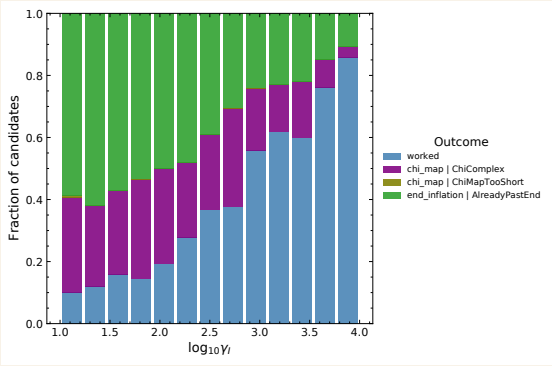

Failure-mode composition in the low-γ_I tail.

Real branch: response to $\bar{\gamma}$

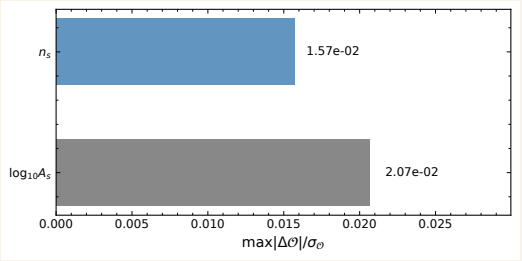

Planck-normalized response of n_s and $\log_{10} A_s$.

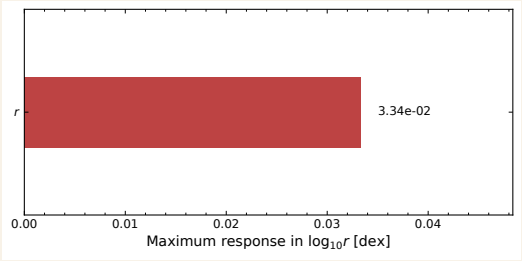

Response of the tensor amplitude, shown as a shift in $\log_{10} r$.

Real branch:$\bar{\gamma}$ posterior

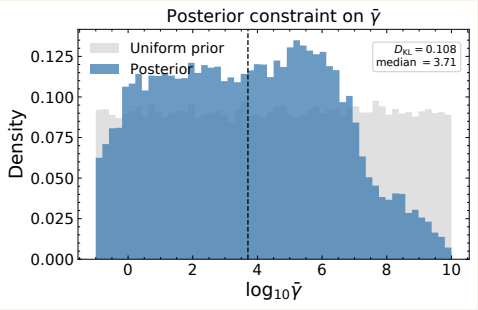

Posterior distribution of $\log_{10}\bar{\gamma}$.

Real branch: $\bar{\gamma}$ posterior

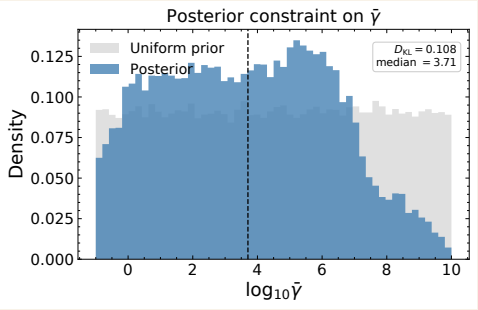

Posterior distribution of $\log_{10}\bar{\gamma}$.

$\bar{\gamma}$ tail tests

- Uniform tests near the posterior drop indicate that almost all sampled real-$\bar{\gamma}$ candidates remain successful, apart from isolated failures.
- This suggests local stability of the real branch in the posterior-supported region.
- A plausible interpretation is that MCMC moves away from regions disfavored by the combined likelihood and viability filters.
- The random tail test therefore probes the neighborhood selected by the posterior, rather than the full high-$\bar{\gamma}$ prior tail.
- Further resolution would require additional exact Mathematica evaluations, especially near boundaries between successful and failed trajectories.

CMB observables: the upcoming constraint

Post-inflationary evolution

Two coupled fluids: an inflaton component and a radiation bath.

$$\dot{\rho}_\phi + 3H(1+w)\rho_\phi = -\Gamma\rho_\phi$$

$$\dot{\rho}_{\rm rad} + 4H\rho_{\rm rad} = \Gamma\rho_\phi$$

$$3M_{\rm Pl}^2 H^2 = \rho_\phi + \rho_{\rm rad}$$

w: the effective equation-of-state parameter

Γ: the constant dissipation rate

2510.27587v2

CMB observables: the upcoming constraint

Post-inflationary evolution

Two coupled fluids: an inflaton component and a radiation bath.

$$\dot{\rho}_\phi + 3H(1+w)\rho_\phi = -\Gamma\rho_\phi$$

$$\dot{\rho}_{\rm rad} + 4H\rho_{\rm rad} = \Gamma\rho_\phi$$

$$3M_{\rm Pl}^2 H^2 = \rho_\phi + \rho_{\rm rad}$$

w: the effective equation-of-state parameter

Γ: the constant dissipation rate

2510.27587v2

Crossing condition

Reheating temperature identified with the radiation temperature

$$\rho_{\rm rad}(t_{\rm re}) = \rho_\phi(t_{\rm re})$$

$$\rho_{\rm rad}(t_{\rm re}) = \frac{\pi^2}{30}\, g_*(T_{\rm re})\, T_{\rm re}^4.$$

CMB observables: the upcoming constraint

Post-inflationary evolution

Two coupled fluids: an inflaton component and a radiation bath.

$$\dot{\rho}_\phi + 3H(1+w)\rho_\phi = -\Gamma\rho_\phi$$

$$\dot{\rho}_{\rm rad} + 4H\rho_{\rm rad} = \Gamma\rho_\phi$$

$$3M_{\rm Pl}^2 H^2 = \rho_\phi + \rho_{\rm rad}$$

w: the effective equation-of-state parameter

Γ: the constant dissipation rate

2510.27587v2

Crossing condition

Reheating temperature identified with the radiation temperature

$$\rho_{\rm rad}(t_{\rm re}) = \rho_\phi(t_{\rm re})$$

$$\rho_{\rm rad}(t_{\rm re}) = \frac{\pi^2}{30}\, g_*(T_{\rm re})\, T_{\rm re}^4.$$

General strategy

$$U(\phi;\Theta) \implies (n_s(\Theta), A_s(\Theta), r(\Theta))_{k_*}$$

$$\overset{\rm CMB}{\Longrightarrow} \quad \Theta \text{ restricted.}$$

$$\implies \quad T_{\rm re}$$

Application to the left–right Higgs-inflation model

Application

In the large-field regime, the single-field trajectory gives a plateau potential of the same qualitative class as an E-model:

$$U(\chi) \simeq U_0 \left(1 - 2e^{-2\sqrt{(\zeta+\eta)}\chi/M_{\rm Pl}}\right).$$

For inflaton, χ, the leading plateau scale is controlled by

$$U_0 \sim \frac{\lambda M_{\rm Pl}^4}{(\zeta+\eta)^2}.$$

Application to the left–right Higgs-inflation model

Application

In the large-field regime, the single-field trajectory gives a plateau potential of the same qualitative class as an E-model:

$$U(\chi) \simeq U_0 \left(1 - 2e^{-2\sqrt{(\zeta+\eta)}\chi/M_{\rm Pl}}\right).$$

For inflaton, χ, the leading plateau scale is controlled by

$$U_0 \sim \frac{\lambda M_{\rm Pl}^4}{(\zeta+\eta)^2}.$$

CMB data

- The scalar observables already restrict combinations such as

$$q = \zeta + \eta, \qquad u = \log_{10}(\lambda/q).$$

Application to the left–right Higgs-inflation model

Application

In the large-field regime, the single-field trajectory gives a plateau potential of the same qualitative class as an E-model:

$$U(\chi) \simeq U_0 \left(1 - 2e^{-2\sqrt{(\zeta+\eta)}\chi/M_{\rm Pl}}\right).$$

For inflaton, χ, the leading plateau scale is controlled by

$$U_0 \sim \frac{\lambda M_{\rm Pl}^4}{(\zeta+\eta)^2}.$$

CMB data

- The scalar observables already restrict combinations such as

$$q = \zeta + \eta, \qquad u = \log_{10}(\lambda/q).$$

- They do not strongly distinguish the real and imaginary $\bar{\gamma}$ sectors.

Application to the left–right Higgs-inflation model

Application

In the large-field regime, the single-field trajectory gives a plateau potential of the same qualitative class as an E-model:

$$U(\chi) \simeq U_0 \left(1 - 2e^{-2\sqrt{(\zeta+\eta)}\chi/M_{\rm Pl}}\right).$$

For inflaton, χ, the leading plateau scale is controlled by

$$U_0 \sim \frac{\lambda M_{\rm Pl}^4}{(\zeta+\eta)^2}.$$

CMB data

- The scalar observables already restrict combinations such as

$$q = \zeta + \eta, \qquad u = \log_{10}(\lambda/q).$$

- They do not strongly distinguish the real and imaginary $\bar{\gamma}$ sectors.

Next elimination step: Use the inferred endpoint of inflation and a reheating prescription to compute

$$T_{\rm re} = T_{\rm re}(n_s, A_s, r;\, w, \Gamma).$$

The way forward

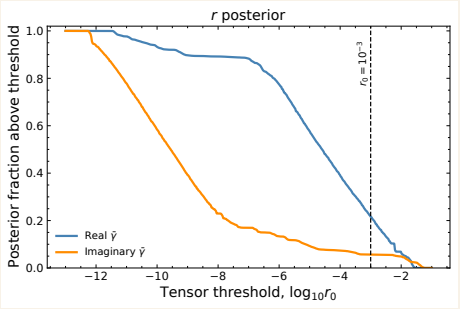

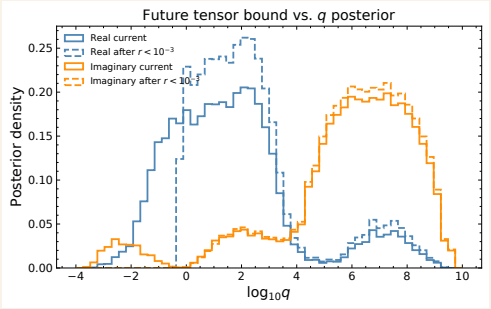

A null result at $r < 10^{-3}$ would not exclude either branch: 78.4% of the real branch and 94.4% of the imaginary branch remain viable.
Potential constraint on high-r tail of the real-$\bar{\gamma}$ posterior.

Backup slides

Backup: posterior structure, imaginary branch

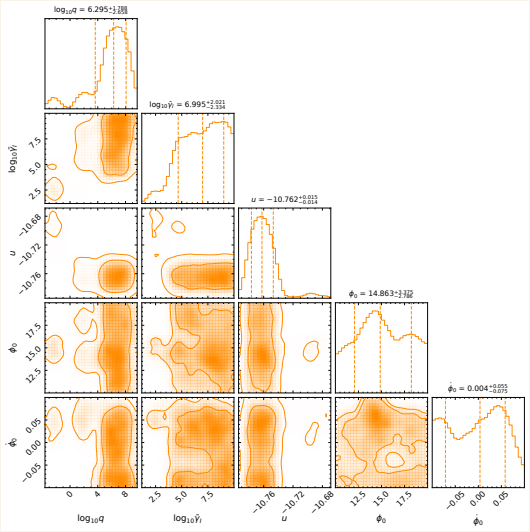

Backup: posterior structure, real branch

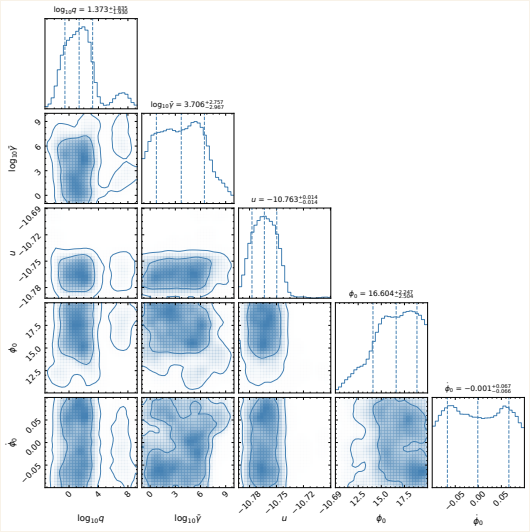

Backup: regressor feature importance, imaginary branch

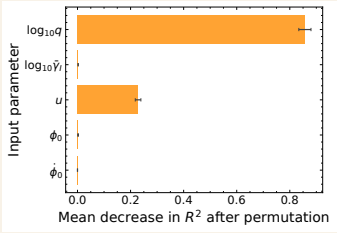

n_s regressor

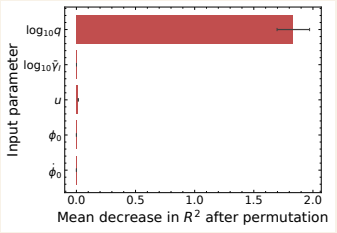

$\log_{10} r$ regressor

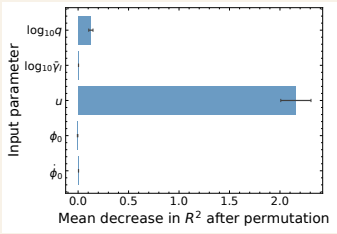

$\log_{10} A_s$ regressor

Backup: regressor feature importance, real branch

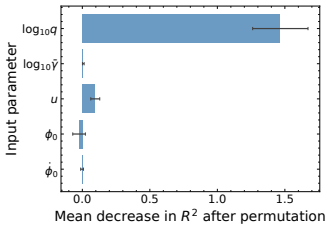

n_s regressor

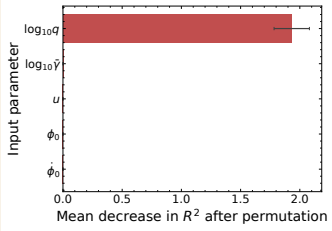

$\log_{10} r$ regressor

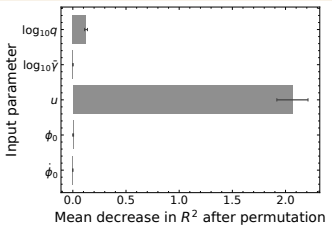

$\log_{10} A_s$ regressor

Alternative first-order quantization: role of $\bar{\gamma}$

First-order quantization

Alternatively: keep the tensor phase-space pair

$$(h_{ij}, B_{ij})$$

and quantizes before eliminating the connection variable.
In this route, $\bar{\gamma}$ can re-enter through the canonical variables, Hamiltonian ordering, and reality conditions.
For imaginary $\bar{\gamma}$, this can induce a chiral asymmetry between left- and right-helicity graviton spectra.

1104.1800

constant-$\bar{\gamma}$ approximation

$$\gamma(\phi_0) = \bar{\gamma}.$$

$$\gamma(\phi) = \bar{\gamma}\,\frac{1 + q\phi^2}{\left(\frac{1}{\phi_0^2} + q\right)\phi^2}$$

Along representative viable trajectories, the fractional variation of $\gamma(\phi)$ during inflation is negligible, $\Delta_\gamma \lesssim 2.5 \times 10^{-7}$. Hence the constant-$\bar{\gamma}$ first-order quantization picture can be used.